

Exclusive Study of Deuteron Electrodisintegration near Threshold

G.D. Cates, R. Lindgren, N. Liyanage, V. Nelyubin, B. E. Norum**,
K. Paschke, L.C. Smith, R. Subedi, K. Wang*, X. Zheng

University of Virginia, Charlottesville, VA

W. Bertozzi*, S. Gilad*, B. Moffit, N. Sparveris
MIT, Cambridge, MA

H. Arenhövel
University of Mainz, Mainz, Germany

M. Schwamb
ECT, Trento, Italy*

B. Sawatzky
Temple University, Philadelphia, PA

S. Širca,
University of Ljubljana, Ljubljana, Slovenia

R. Igarashi, R. Pywell
University of Saskatchewan, Saskatoon, Canada

J.R.M. Annand, D. Ireland, J. Kellie, K. Livingston

G. Rosner, D. Watt
University of Glasgow, Glasgow, Scotland, UK

X. Jiang
Rutgers University, New Brunswick, NJ

J. Calarco
University of New Hampshire, Durham, NH

Y. Jiang, H. Lu, J. Shen, X. Yan, Y. Ye, Z. Yin, P. Zhu
University of Science. and Technology, Hefei, China

J. P. Chen, J.-O. Hansen, D. W. Higinbotham, J. LeRose, V. Sulkosky
Jefferson Laboratory, Newport News, VA

and
the Hall A Collaboration

Abstract

Elastic electron scattering from the deuteron and near-threshold electrodisintegration have long provided benchmarks against which models of the nucleon-nucleon interaction are evaluated. Recent measurements of T_{20} in elastic scattering have tightened the constraints but still leave room for ambiguity. We propose to make similar improvements in the constraints imposed by electrodisintegration with an exclusive study of the reaction $d(\vec{e}, e'p)n$ at $Q^2 = 12 \text{ fm}^{-2}$ and $E_{np} = 2, 4, 6, 8 \text{ MeV}$. Under these kinematics, non-nucleonic as well as nucleonic degrees of freedom and relativistic effects are expected to play major roles. The experiment will be conducted in Hall A at JLab using the polarized CW electron beam, an HRS spectrometer to detect the electron, and the BigBite spectrometer to detect the proton. The first part of the experiment will be to extract the structure functions f_{LT} , f_{TT} , and f'_{LT} at an electron beam energy of 3200 MeV and electron scattering angle of 12.5° . The second part of the experiment will be to separate the longitudinal and transverse structure functions, f_L and f_T , by performing complementary measurements with a beam energy of 550 MeV and electron scattering angle of 90° . The individual structure functions are expected to be particularly sensitive to different components of the interaction. For example, f_{LT} is expected to be sensitive to relativistic effects, f_T is expected to be dominated by MEC effects, and f'_{LT} vanishes unless final state interactions are present and is expected to be insensitive to non-nucleonic degrees of freedom. The longitudinal cross section for elastic scattering depends on the isoscalar charge current whereas f_L for electrodisintegration depends primarily on the isovector charge current. Comparison of the two, as measured at the same time will allow us to separate the two contributions. A comparison of these data with theoretical models will isolate individual interaction components and thus provide more stringent tests of calculations.

This experiment was approved by PAC 22 in July, 2002, subject to the condition that we demonstrate that the experiment can be run at within a factor of two of the proposed luminosity. The specific concern was the singles rate in the BigBite spectrometer. Reasonable extrapolations from experiments conducted since then have demonstrated that the luminosity proposed here can be used with adequate detection efficiencies and track reconstruction efficiencies.

1 Introduction

The defining goal of nuclear physics is to understand the composition and dynamics of nuclei in terms of their constituents. A first step towards this goal is to understand the interaction between nucleons. As the only stable two-nucleon system, the deuteron is the ideal choice to study this interaction. Electrodisintegration is an excellent probe for several reasons. First, the fundamental interaction is well-understood and weak. Second, the structure functions describing electrodisintegration are functions of both Q^2 , the 4-momentum transfer, and W , the invariant mass of the two-nucleon system. The dependencies of the structure functions on Q^2 and W are differentially sensitive to various aspects of the physics involved. By investigating a particular region of the $Q^2 - W$ plane one can examine specific aspects of the physics involved. Third, by using a polarized electron beam and measuring the momentum of the ejected proton it is possible to isolate individual structure functions. Such detailed information will yield an even greater insight into the physics of the deuteron.

Elastic electron scattering from the deuteron and near-threshold electrodisintegration have long been a testing ground for models of the nucleon-nucleon interaction. Measurements of T_{20} in elastic scattering have tightened the constraints but still leave room for ambiguity. We propose to further tighten these constraints through simultaneous measurements of the reactions $d(e, e'd)$ and $d(\vec{e}, e'p)n$ near threshold at $Q^2 = 12 \text{ fm}^{-2}$. Under these kinematics, non-nucleonic as well as nucleonic degrees of freedom and relativistic effects are expected to play major roles.

The potential significance of these studies was highlighted at the PAC14 Few-Body Workshop [1]. There, the first of three “Key Questions” was identified as ‘Can few-body systems be understood in terms of a “*standard model*” for nuclear physics with only nucleon degrees-of-freedom?’ Under this the first three key issues were identified as

- Is a consistent and “exact” description of ${}^2\text{H}$, ${}^3\text{H}$, ${}^3\text{He}$, and ${}^4\text{He}$ possible within a standard model? (i.e. can a single interaction and current operator account for all nuclei?)

- Precise and complete tests of the “*standard model*” need to be identified and carried out experimentally.
- A complete “*standard model*” requires correct incorporation of relativistic effects, meson-exchange currents, and isobar currents.

In looking to a program of measurements to address these issues the first item listed under “Experimental Opportunities for the Future” was “*Threshold deuteron electrodisintegration: Measurements of this reaction at Jefferson Lab could extend the exploration of the role of meson-exchange currents to higher momentum transfer.*” While the current proposal does not focus on the highest momentum transfers possible, it does address directly both the nucleonic and non-nucleonic currents in the deuteron. Thus, the proposed measurements constitute the first step on this important path.

In the case of unpolarized beam and target, the coincidence cross section contains four dynamical functions, the longitudinal (f_L), transverse (f_T), transverse-transverse (f_{TT}), and the longitudinal-transverse (f_{LT}) interference terms. A fifth structure function (f'_{LT}) will be involved when a polarized electron beam is used. Earlier studies showed the strong sensitivity of deuteron electrodisintegration to non-nucleon degrees of freedom. Therefore, it is an important step to study in detail effects such as meson-exchange currents (MEC) and isobar configuration (IC), as well as relativistic corrections (RC) to the structure functions. From the theoretical side, these interaction effects can be cleanly investigated in the two-nucleon system since there are no problems arising from many-particle effects.

Inclusive data [2] on the reaction $d(e, e')pn$ near threshold showed that almost 100% of the experimental cross section near $Q^2 = 12 \text{ fm}^{-2}$ can be accounted for by the inclusion of MECs. While this established that non-nucleonic degrees of freedom are important, the availability of only cross section data limits the interpretive and thus predictive power of the calculations. The MECs are expected to be particularly important to the transverse structure function f_T so extracting f_T will be one of the most important foci of the proposed work. A precise determination of f_T as a function of θ_p , the angle at which the proton emerges in the center of mass system, and E_{np} (the relative energy of the neutron and proton in the final state) will place tight

constraints on models of non-nucleonic effects.

The structure functions f_T and f_L will be extracted via a Rosenbluth separation. The function f_L will provide us an opportunity to study the isovector charge contribution. This will be the second major focus of the experiment. While the transverse component has been extensively studied by backward angle electron scattering, the longitudinal term has been largely ignored; extracting it requires a precise L/T separation. The high energy CW beam at Jlab and the high resolution HRS spectrometer makes such a separation feasible.

It was found from theoretical calculations [3] [4] and from data [5] [6] [7] that the longitudinal-transverse component f_{LT} is specifically sensitive to RCs. It was also shown [4] that relativistic effects become visible above $Q^2 = 5 fm^{-2}$ and increase with the momentum transfer. Close to the quasi-elastic (QE) region the relativistic two-body contribution is small, but the effect increases as one moves away from QE kinematics. Since most of the previous data were obtained in the QE region and at low Q^2 , measurements near threshold and at higher Q^2 will enable us to observe a sizable contribution from relativistic effects. The importance of understanding relativistic effects is clear; it will pave the way for searching for a quark-gluon signature in future investigations at higher Q^2 . This will be the third major focus of our experiment.

With the polarized electron beam, the fifth structure function f'_{LT} can be obtained. The function f'_{LT} vanishes in plane wave approximation, so a finite f'_{LT} will enable us to study final state interactions (FSI) if for no other reason than to account for their effects in our measurements of the other structure functions.

To date, few measurements of either photo- or electrodisintegration of the deuteron near threshold have been made. Total, unpolarized photodisintegration cross sections for $E_\gamma \approx 2.75$ MeV [8], corresponding to $E_{np} \approx 0.5$ MeV, have been measured, as have differential cross sections (at selected θ_n) for $E_\gamma \leq 20$ MeV [8]. Measurements of $d(\gamma, \vec{n})$ for $E_\gamma = 2.75$ MeV and a variety of neutron angles as well as for a variety of energies $E_\gamma \leq 35$ MeV and a neutron angle of 90° have also been made [9]. During the last few years, a UVA/Saskatchewan/Duke collaboration has measured the reaction $d(\vec{\gamma}, n)p$

at $E_\gamma = 3.5, 4.0, 6.0, 10.0, 14.0,$ and 16.0 MeV corresponding to $E_{np} = 1.3, 1.8, 2.8, 4.8, 6.8,$ and 7.8 MeV [10, 11]. One recent electrodisintegration measurement close to threshold was made at Darmstadt with $E_{np} \approx 8 - 16$ MeV and Q^2 near 0.07 fm^2 [12].

The kinematics of the threshold electrodisintegration reaction are almost identical to those of elastic scattering so we will observe simultaneously electrons scattered elastically from the deuteron. The very large momentum acceptance of the BigBite spectrometer will enable us to measure the momentum of the recoiling deuteron as well. Time-of-flight and E-dE cuts will enable us to distinguish them cleanly from protons. Thus, we will measure the two reactions under the same conditions, making possible precise comparisons.

In summary, we propose an out-of-plane measurement of deuteron electrodisintegration in Hall A at $Q^2 \approx 12 \text{ fm}^{-2}$ near threshold ($E_{np} = 2$ to 8 MeV), where MEC, IC, and RC effects are expected to be eminent and distinguishable. The Q^2 chosen corresponds to a minimum in the cross section as calculated without non-nucleonic effects, thus these effects can be magnified. The momentum transfer Q^2 is high enough to investigate these effects while low enough to avoid involving quark-gluon effects. The experiment consists of two parts. The data measured using $E = 3200$ MeV will be used to extract the three interference structure functions, f_{LT}, f_{TT}, f'_{LT} , as well as a sum of the longitudinal and the transverse cross sections. The data measured using $E = 550$ MeV will be used in combination with the data taken at $E = 3200$ MeV to separate the longitudinal and transverse structure functions, f_L and f_T . The particular sensitivity of f_L to the isovector charge currents, that of f_T to MECs, that of f_{LT} to RCs, and that of f'_{LT} to FSI will enable us to test existing models of the nucleon-nucleon interaction and to rigorously constrain future calculations. We also will gather precise data on deuteron elastic scattering with longitudinal (σ_L) and transverse cross section (σ_T) separated.

2 Previous Data

Over the past forty years there have been many studies of deuteron electrodisintegration, mostly by means of inclusive measurements. Starting in 1962 [13] at $Q^2 = 0.16 fm^{-2}$ the measurements were extended to $28 fm^{-2}$ in 1985 [2] and to $40 fm^{-2}$ in 1991 [14] [15]. The high Q^2 measurements were performed at backward angles and involved the interaction of transverse virtual photons with the current and magnetization densities of the deuteron. Within a few MeV of threshold, the M1 transition from the isospin singlet ${}^3S_1 + {}^3D_1$ ground state to the final scattering state, isospin triplet 1S_0 , dominates the cross section. Near $Q^2 = 12 fm^{-2}$, the plane wave impulse approximation reaches a deep minimum due to the destructive interference between ${}^3S_1 \rightarrow {}^1S_0$ and ${}^3D_1 \rightarrow {}^1S_0$ transition [2]. The filling in of this dip by the inclusion of MEC constituted a major step forward in our theoretical understanding of nucleon interactions.

Coincidence measurements on the deuteron were performed at Kharkov [16] [17] and Saclay [18]. They were all in coplanar kinematics and no attempt was made to dissect the cross section. The measurement of coincidence cross sections for deuteron electrodisintegration in out-of-plane kinematics was pioneered by Tamae *et al.* at Sendai [19] for $Q^2 = 0.11 fm^{-2}$ and $E_{np} = 18 MeV$. The two interference terms and the sum of longitudinal and transverse terms were studied. The results were in good agreement with theoretical calculations based on the Paris potential.

A proposal for coplanar measurements [20] at $Q^2 = 8.7 fm^{-2}$ was approved at the MIT-Bates Laboratory. Unfortunately, due to the decommissioning of the MEPS spectrometer, the project was canceled. At Bonn, data for f_{LT} was obtained at $Q^2 = 4.5 fm^{-2}$ and $E_{np} = 15 MeV$ [21]. One measurement of the fifth structure function in the QE region at $Q^2 = 3.3 fm^{-2}$ was performed at the MIT-Bates Laboratory [22], but it suffered from large uncertainties. Another measurement conducted at the MIT-Bates Laboratory with $E_e = 800 MeV$ and $Q^2 = 3.8 fm^{-2}$ [23] focused on the dip region below the Δ peak. The interference terms and the fifth structure functions were obtained, clearly revealing strong evidence for RCs and FSIs. There are also data sets from NIKHEF in the QE and Δ -regions [24] [25]. These data are summarized in

Table 1. Most of these data are either near the QE or Δ regions and are at lower momentum transfers. There is no uniform set of data from which all the five structure functions have been extracted. Since most of these data were taken with low-duty factor beam, the statistical precision was, in general, poor.

The MIT data at 3.8 fm^{-2} [26] showed an agreement with theory on f_T , while the f_L data were 25% lower than calculation. On the other hand, the MIT data of f_T agreed with the NIKHEF data [24], but f_L differed 40%. Apparently, the longitudinal component is less understood in both theory and experiment. As for f_{LT} , the NIKHEF data [6] showed a signature of relativistic corrections, while similar data from Saclay [27] can be fit by a non-relativistic calculation. These discrepancies observed in the QE region could be clarified by pushing the measurements to higher Q^2 and to the threshold region, where the interaction effects are anticipated to be stronger.

Most recently, an out-of-plane measurement of the reaction ${}^2H(e, e'p)n$ near threshold was carried out at Darmstadt using an electron energy of 85 MeV and scattering angle of 40° corresponding to a Q^2 of 0.07 fm^{-2} . Protons corresponding to $E_{np} = 8\text{-}16 \text{ MeV}$ [12] were detected at $\phi_p = 0, 45, 135, \text{ and } 180^\circ$. While it was found that the data on $\sigma_L + \sigma_T$ are in good agreement with the calculations of Arenhövel *et al.* when the proton is emitted parallel to \vec{q} ($\theta_p < 75^\circ$), they lie a factor of two above the calculation in the minimum near $\theta_p \approx 85^\circ$ and 30-40% below the calculation for $\theta_p > 150^\circ$. The data on σ_{LT} lie about 40% below the calculations for $\theta_p \approx 40^\circ$ where σ_{LT} goes maximally negative; the data for $\theta_p > 150^\circ$ point to a similar discrepancy where σ_{LT} is positive.

That such large discrepancies exist at such low Q^2 where we expect calculations to be valid strongly suggests that our understanding of the deuteron is far from complete, that it may be far poorer than we generally believe. A systematic, out-of-plane study of near threshold electrodisintegration carried out under kinematics where all relevant degrees of freedom play significant roles and paired with a simultaneous measurement of elastic scattering promises to be the best way to clarify these issues.

Existing data on threshold electrodisintegration in the range of Q^2 of interest

are shown in figure 1. These data represent measurements integrated over the proton emission angle for values of $E_{np} \leq 3.0 \text{ MeV}$. The data near $Q^2 = 12 \text{ fm}^{-2}$ have uncertainties of about $\pm 10\%$. The data below $Q^2 = 12 \text{ fm}^{-2}$ are consistent at the $\leq 10\%$, following a uniform exponential slope. The data above $Q^2 = 12 \text{ fm}^{-2}$ are consistent at a similar level and follow an identical slope. However, they are displaced by about 30% from the exponential line fit to the lower Q^2 data. No data wherein the dependence of the cross section on proton emission angle has been extracted exist in this range of Q^2 .

Threshold photodisintegration results pose similar questions. while measurements of the unpolarized total and differential cross sections are reasonably well reproduced by theoretical calculations, those involving polarization degrees of freedom are not [9]. The neutron induced polarizations observed in the reaction $d(\gamma, \vec{n})$ at $\theta_n = 90^\circ$ appear to agree reasonably with theory below $E_\gamma \leq 10 \text{ MeV}$. However, more extensive measurements over a wider range of θ_n for $E_\gamma = 2.75 \text{ MeV}$ generally disagree by about 40% at neutron emission angles of around 45° and 135° . The data on the reaction $d(\vec{\gamma}, n)$ also show nontrivial disagreement with potential model calculations. The origins of these discrepancies is under investigation but at this point they remain mysteries.

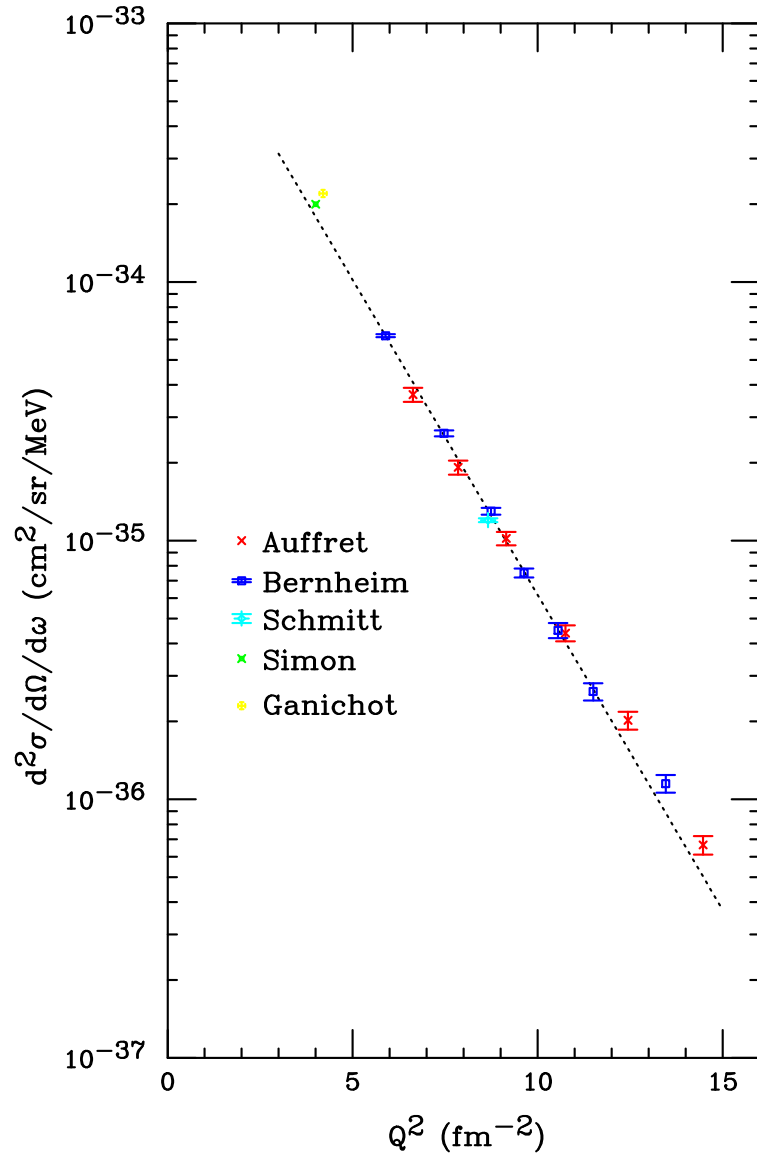


Figure 1: Existing data reported by Auffret *et al.* [2], Bernheim *et al.* [18], Schmitt *et al.* [15], Simon *et al.* [28], and Ganichot *et al.* [29] on the reaction $d(e, e'p)n$ near threshold in the momentum transfer range of interest for the proposed experiment. In each case the angle of emission of the proton is summed over. The cross section is integrated from threshold to $E_{np} = 3 \text{ MeV}$. The dotted line is an exponential fit to the data below $Q^2 = 12 \text{ fm}^{-2}$.

Lab.	Q^2 (fm^{-2})	Region	Goal	Ref.
Kharkov	4.1	QE	$p_N, d\sigma$	[16]
Kharkov	7.2	QE	p_N	[17]
Saclay	1.66	Δ	$d\sigma$	[18]
Saclay	11	QE	L,T,LT	[27]
Sendai	0.11	Thrs	L+T,LT,TT	[19]
Bonn	4.5	Δ	$d\sigma$	[30]
Bonn	3.7	QE	LT	[7]
Bonn	3.1	Δ	$d\sigma$	[21]
NIKHEF	7	QE	L,T	[31]
NIKHEF	5.4	QE	L,T,LT	[24]
NIKHEF	0.77	Δ	TT	[25]
NIKHEF	5.15	QE	LT, $d\sigma$	[6]
Bates	3.8	QE	L,T,LT	[26]
Bates	3.3	QE	LT'	[22]
Bates	3.86	Dip	LT,TT,LT'	[23]
Bates	5.15	QE	LT,TT,LT'	[32]
Mainz	9.3	QE- Δ	p_m	[33]
Mainz	2-4	Dip	L,T	[34]
SLAC	>30	QE	p_m	[35]
Darmstadt	0.07	Thrs	L+T, LT	[12]

Table 1: Previous data from coincidence measurements of deuteron electrodisintegration, p_N and p_m represent the nucleon momentum and missing momentum respectively.

3 Scientific Motivation

3.1 Theoretical Development

Early theoretical work on exclusive deuteron electrodisintegration was carried out by Fabian and Arenhövel [36], within a non-relativistic framework including MEC and IC. The T -matrix was calculated in a multipole expansion up to $L=6$ (including the FSI) while for all higher multipoles the Born approximation for the final-state was used. The calculated cross sections are in good agreement with inclusive data for $0 < Q^2 < 20 fm^{-2}$.

In [37], Arenhövel reported an interpretation of the $d(e,e'p)$ data from Saclay [38] in which FSI, MEC and IC were studied. The effects turned out to be very important except for the QE region. Taking into account these effects led to a satisfactory agreement with experiment, whereas the Born or impulse approximation failed to give even a fair description.

Laget's calculation [39] included FSI and MEC. His analysis of existing data provided strong constraints on the high momentum part of the wave function of the few-body system. The corrections to the impulse approximation are affected by gauge invariance and reproduce a wide range of data obtained under very different kinematic conditions. He emphasized that a more accurate determination requires a significant increase of the duty factor and extension of the study to higher momentum.

Relativistic aspects of the theoretical approaches were explored by Cambi, Mosconi and Ricci [40] [41]. They concluded that although relativistic corrections to the charge density in deuteron photodisintegration are important, these have not been examined for electron scattering experiments, yet.

Mosconi and Ricci [3] studied the effects of nucleonic and pionic relativistic corrections on the structure functions for the $d(\vec{e}, e'p)n$ reaction in the QE region. The functions f_L , f_{LT} , and f'_{LT} show remarkable variations in forward and backward directions.

Observables originating from polarized electron and polarized target were

investigated by Arenhövel *et al.* [42] within a non-relativistic framework, but with lowest order relativistic contributions to the one-body current. The structure functions and the asymmetries corresponding to the various nucleon polarization components were studied with respect to their sensitivity to the potential model, subnucleonic degrees of freedom, and relativistic effects in different kinematic regions.

A thorough relativistic analysis of both elastic electron scattering from the deuteron and electrodisintegration of the deuteron has been performed by J. A. Tjon *et al.* [43]. Their calculations are based on a relativistic covariant field theoretical Bethe-Salpeter equation approach and contain a consistent relativistic treatment of both the electromagnetic current and nucleon-nucleon interaction. Contributions from meson exchange currents including $\rho\pi\omega$ and $\omega e\gamma$ are incorporated.

Recently, a consistent treatment of relativistic effects in deuteron electrodisintegration was systematically investigated in various regions of energy and momentum transfer by Ritz *et al.* [4]. In this work the equation-of-motion and the unitarily equivalent S-matrix approaches were used. In a (p/M) expansion, all leading order relativistic π -exchange contributions consistent with the Bonn one-boson-exchange potential model are included. In addition, static heavy-meson-exchange currents including boost terms, $\gamma\pi\rho/\omega$ currents, and Δ -isobar contributions were considered. Sizable effects from the various relativistic two-body contributions, mainly from π -exchange, were found in inclusive form factors and exclusive structure functions for a variety of kinematic regions. The variation due to different potential models was examined and the differences were found to be small.

3.2 Kinematics and Cross Section

There are two planes involved in the measurement. One is the scattering plane, defined by the momentum of the scattered electron and the incident beam axis; the other is the reaction plane, defined by the momenta of the virtual photon and the emitted proton, as shown in Fig. 2. The incident (scattered) electron beam energy is E (E'), and the scattering angle θ_e .

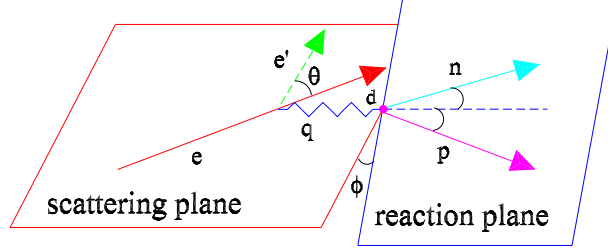


Figure 2: Schematic geometry of the deuteron disintegration reaction. In this figure the incident (scattered) electron is e (e').

The squared four-momentum transfer q^2 carried by the virtual photon is

$$-q^2 = Q^2 = 4EE' \sin^2 \frac{\theta_e}{2},$$

Q^2 is related to the invariant mass of the final state W by

$$W^2 = 2m\nu + m^2 - Q^2,$$

where ν is the energy carried by the virtual photon, m is the mass of the deuteron and

$$\nu = E - E'.$$

The excitation energy or the relative energy of the two nucleon system after the scattering is defined as

$$E_{np} = \Delta W = W - m_p - m_n$$

where m_p and m_n are the mass of proton and neutron respectively.

According to [37], the triply differential cross section for deuteron electrodisintegration can be written as

$$\frac{d^3\sigma}{dE'd\Omega_e d\Omega_p} = C_n(\rho_L f_L + \rho_T f_T + \rho_{LT} f_{LT} \cos \phi_p + \rho_{TT} f_{TT} \cos 2\phi_p +$$

$$h\rho'_{LT}f'_{LT} \sin \phi_p) \quad (1)$$

where $d\Omega_e$ is the differential solid angle subtended by the electron arm in the laboratory frame, and $d\Omega_p$ is for proton in the proton-neutron CM frame with ϕ_p the azimuthal angle of the proton relative to the virtual photon direction;

$$C_n = \frac{\alpha E'}{6\pi^2 Q^4 E},$$

and α is the fine structure constant; $f_{\lambda\lambda'}$ are nuclear structure functions. The kinematic functions $\rho_{\lambda\lambda'}$ describe the polarization density matrix of the exchanged virtual photon, and the virtual photon density matrix is given by [36]

$$\sigma_{\mu'\mu}^{(\gamma)} = \frac{\alpha}{2\pi^2} \frac{E'}{EQ^4} \rho_{\mu\mu'},$$

with $\mu = 0$ for longitudinal and $\mu = \pm 1$ for transverse polarization of the virtual photon. The ratio of ρ_L and ρ_T will be used as relative longitudinal polarization according to

$$\epsilon_L = \frac{\rho_L}{2\rho_T}. \quad (2)$$

In the above expression, f_L and f_T are the transverse and longitudinal structure functions, in principal, they can be separated by choosing two different sets of beam energy and scattering angle at fixed Q^2 and ν . The rest are the interference terms between longitudinal and transverse (f_{LT}), as well as transverse and transverse (f_{TT}). The f'_{LT} term is proportional to the helicity of the electron beam, h , and $\sin\phi_p$. These interference terms are not visible in inclusive measurements, since their contribution cancels in the summation over the azimuthal angle ϕ_p . However, these terms are expected to contain new information about the N-N interaction.

The azimuthal angle dependence of the cross section can be used to separate the interference terms. While f_L , f_T and f_{LT} can, in principal, be determined using coplanar geometry for $\phi_p = 0$ and π , f_{TT} will require an out-of-plane measurement. Similarly, in principal f'_{LT} can be measured at $\phi = 90^\circ$ with $h = 1$ and $h = -1$. However, in order to extract these relatively small quantities with a minimal sensitivity to systematic uncertainties one must perform a measurement with as much out-of-plane acceptance as possible.

3.3 Theoretical Predictions

The aforementioned calculations as well as others not listed give reasonable descriptions of the inclusive cross sections in this range of momentum transfer that have been measured to date. An exclusive measurement will provide a more rigorous test of the model. For the purpose of illustrating the sensitivities of the various observables to the components of the underlying physics we have chosen to focus on the calculations of Arenhövel.

Figs. 3 and 4 show the predictions of Arenhövel [44] for all five structure functions for $E_{np} = 2$ and 6 MeV and $Q^2 = 12 fm^{-2}$. In these figures, the dotted curves represent his “Normal” calculation which is based on the Impulse Approximation (IA) plus FSI; the dashed curves represent Normal+MEC; the dash-dot curves represent Normal+MEC+IC; and the solid represents Normal+MEC+IC+RC.

Since f_L originates with the charge density, it is not expected to be sensitive to MEC. Consequently, in the f_L panels of all two figures the dashed (Normal+MEC) curve lies atop the dotted (Normal) curve (creating a dot-long dash curve). In addition, this calculation sets a scale for the IC contribution to f_L at about 15% and that of the RC at about 6%. The calculation indicates that in our kinematics the IC and RC contributions generate a constant shift of f_L and f_T . Thus, the shape and magnitude of $f_L(\theta_p)$ can provide a sensitive test of the isovector charge current contribution prediction of calculations wherein the isoscalar charge current contribution has been constrained by the elastic scattering results.

Unlike f_L , the f_T is very sensitive to MECs. For $E_{np} = 2$ MeV the MECs generate about 65% of the cross section while ICs and RCs contribute about 20% and 15% respectively. By comparing f_T at different values of E_{np} , one sees that the MEC effects are larger at smaller E_{np} .

One attractive feature of f_{LT} is its selective sensitivity to the relativistic corrections. While MECs and ICs do not make a big change to f_{LT} , the relativistic corrections affect not only the amplitude but also the shape; there is even a sign change near 90° . At $\theta_p = 140^\circ$, RCs increase f_{LT} by 45% for $E_{np}=6$ MeV. In contrast to the effect of MECs on f_T , the effect of RCs on

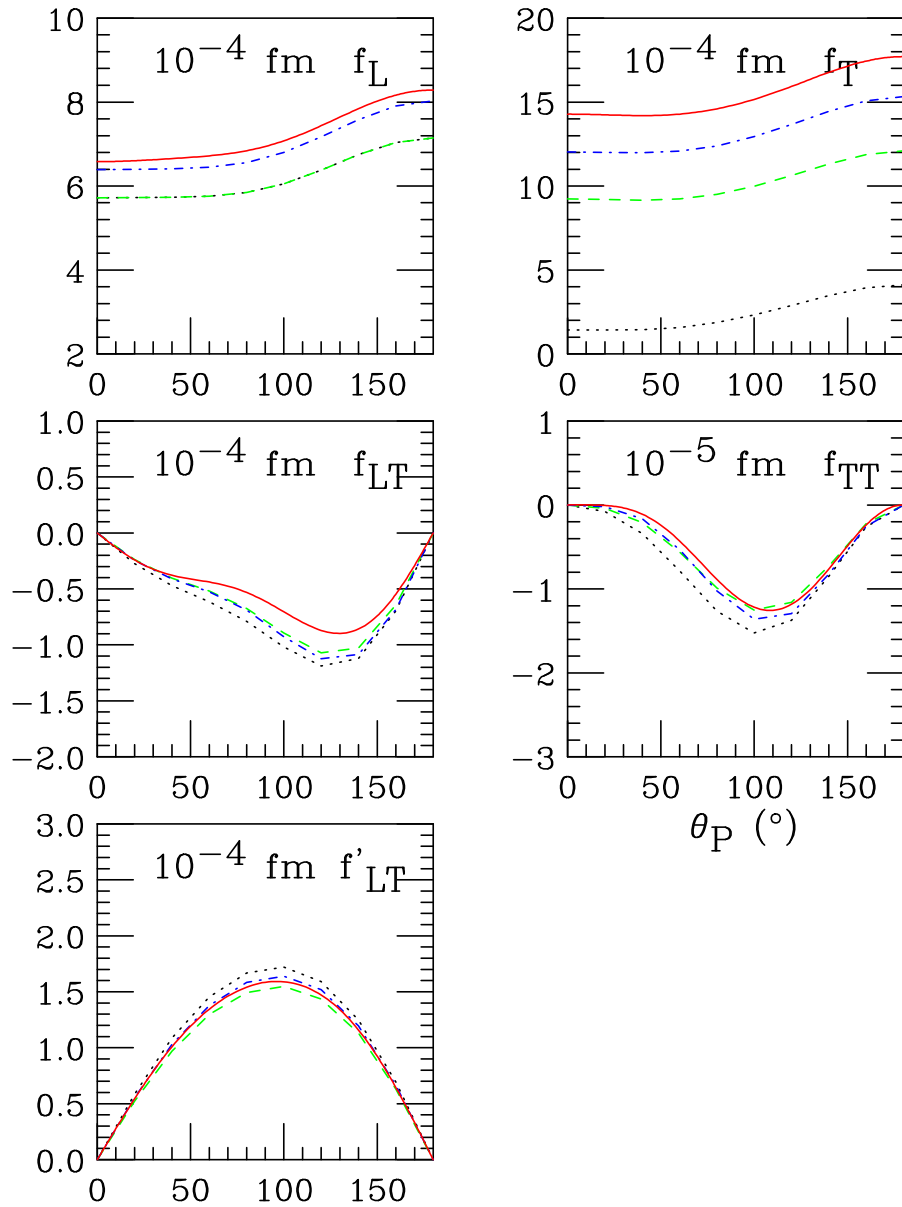


Figure 3: Theoretical structure functions for $Q^2 = 12 \text{ fm}^{-2}$ and $E_{np} = 2 \text{ MeV}$. The dotted (black) curve is for the Normal calculation; the dashed (green) for Normal+MEC; the dash-dotted (blue) for Normal+MEC+IC; and the solid (red) for Normal+MEC+IC+RC. Note that in the f_L plot the dotted and dashed curves are indistinguishable.

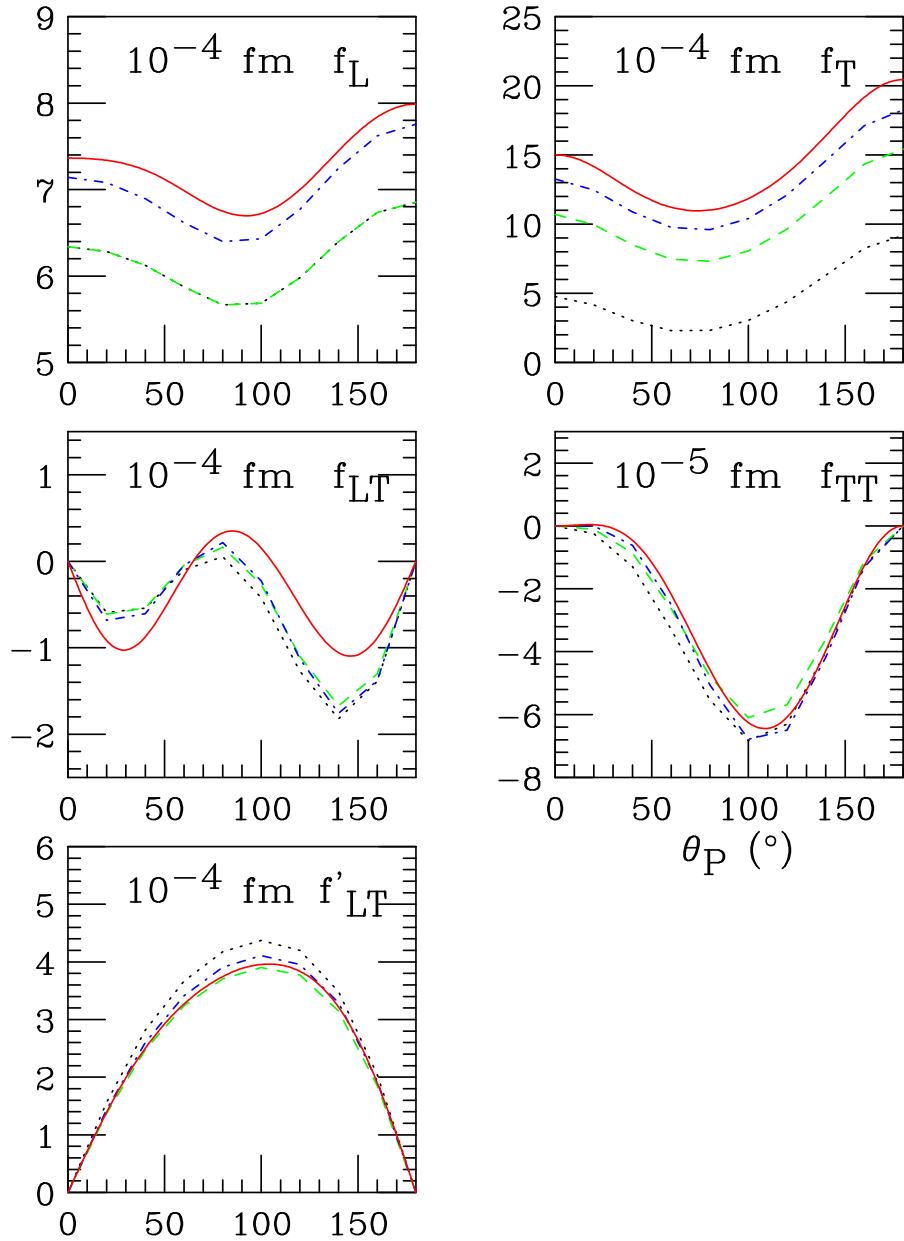


Figure 4: Theoretical structure functions for $Q^2 = 12 \text{ fm}^{-2}$ and $E_{np} = 6 \text{ MeV}$. The dotted (black) curve is for the Normal calculation; the dashed (green) for Normal+MEC; the dash-dotted (blue) for Normal+MEC+IC; and the solid (red) for Normal+MEC+IC+RC. Note that in the f_L plot the dotted and dashed curves are indistinguishable.

f_{LT} increases as E_{np} increases.

In the kinematic region under investigation neither MECs, ICs, nor RCs are computed to have much effect on f_{TT} . However, if Arenhövel's calculations of this observable are reasonably accurate then the amplitude of f_{TT} will be an order of magnitude smaller than that of f_{LT} . Consequently, the error bars for f_{TT} are expected to be larger. It may, nevertheless, be possible to determine the amplitude of this term even if we cannot determine its shape with any precision.

To extract the fifth structure function f'_{LT} , one has to use a polarized electron beam. Since f'_{LT} originates from the imaginary part of the interference between the longitudinal and transverse components, it vanishes in a plane wave calculation as shown in [44]. Moreover, Arenhövel's calculations suggest that f'_{LT} is less sensitive to MECs, ICs and RCs. Therefore, f'_{LT} data will be a direct measure of FSI insofar as we understand the nuclear wave function. The possible uncertainty in our knowledge of the nuclear wave function indicated by the recent results from Darmstadt suggests that our measurements of f'_{LT} and f_{TT} may yield valuable information despite their relatively larger error bars.

While the details of the above discussion are specific to the calculation of Arenhövel, general conclusions can be drawn. First, the previous success of this calculation suggests that it will at least set the scale for the observables to be measured. This gives us confidence that the precision anticipated in the proposed measurements will be adequate to illuminate new physics. Second, the particular sensitivities of the various observables to contributions from the underlying physics derive not from specifics of any one calculation but from more general principles. Consequently, the complementarity of the proposed measurements of a set of observables promises, in a quasi model-independent way, to delineate these contributions.

4 Experiment

4.1 Objectives and Equipment

The proposed experiment will measure all five structure functions simultaneously at four values of E_{np} . Due to their selective sensitivities, each structure function will illuminate a different aspect of the underlying physics.

We will employ one HRS to detect the scattered electrons and the BigBite spectrometer to detect the recoiling protons (as well as recoiling deuterons from elastic scattering events). The high resolution of the HRS will allow a precise determination of W (hence E_{np}) and \vec{q}_3 . The large acceptance of the BigBite will subtend a large fraction of the forward-emitted protons along \vec{q}_3 . The liquid deuterium target cell will be 6 cm long and 1 inch in diameter with 5 mil thick 7075 aluminum end caps and side wall. A snout extending towards the target minimizes the area and hence the thickness of the entrance window to the helium bag which precedes the first detector. The experimental configuration will be essentially the same as for the upcoming experiment to measure threshold π^0 electroproduction from the proton (E04-007 [45]).

It is currently planned to run the experiment with the BigBite spectrometer on the right side of the beamline and to use the LHRS to detect the electrons. To minimize the time required for changes of the BigBite angle it is planned to move the RHRS to its largest possible angle and have the BigBite always forward of it. There is some possibility that this may not be possible when the BigBite is at the largest planned angle of 77.8° as it may collide with the RHRS. If this turns out to be the case then we can run the experiment with the BigBite spectrometer on the left side, using the RHRS to detect the electrons. This is possible because the energies of the electrons to be detected will not exceed 3200 MeV.

4.2 BigBite and HRS Spectrometers

The device which makes this experiment feasible is the non-focusing BigBite spectrometer with its large solid angle (96 msr) and large momentum bite (200-900 MeV/c). The important parameters of this device and HRS are given in Table 2. Its central element is a non-focusing dipole magnet. The detector system to be used when the spectrometer is used to analyze hadrons consists of two three-plane MWPCs and fast scintillator planes with which accurate timing ($\sigma=0.75$ ns) will be obtained.

The two MWPCs have active areas of 1400×350 mm² and 2000×500 mm², respectively, and contain 2600 sense wires in total. The sense wires in the two chambers are separated 1 cm. One plane of wires is tilted at $+60^\circ$, the second at -60° , and the third horizontally.

	HRS	BigBite
p-range (MeV/c)	300-4000	200-900
acceptance_H (mrad)	± 20	± 80
acceptance_V (mrad)	± 60	± 300
solid angle (msr)	4.8	96
δ p/p	10^{-4}	5×10^{-3}
$\delta\theta_H$ (mrad)	0.6	3.2
$\delta\theta_V$ (mrad)	2.0	3.2
measure	\vec{p}_e , vertex	\vec{p}_p , vertex
σ_{vertex} (cm)	0.064	0.32
focusing	$\langle x \theta \rangle = 0$	none

Table 2: Comparison of HRS and BigBite.

4.3 Kinematics

To separate the transverse (f_T) from the longitudinal (f_L) components, we need to take data at two different ($E - \theta_e$) settings while Q^2 and E_{np} are kept

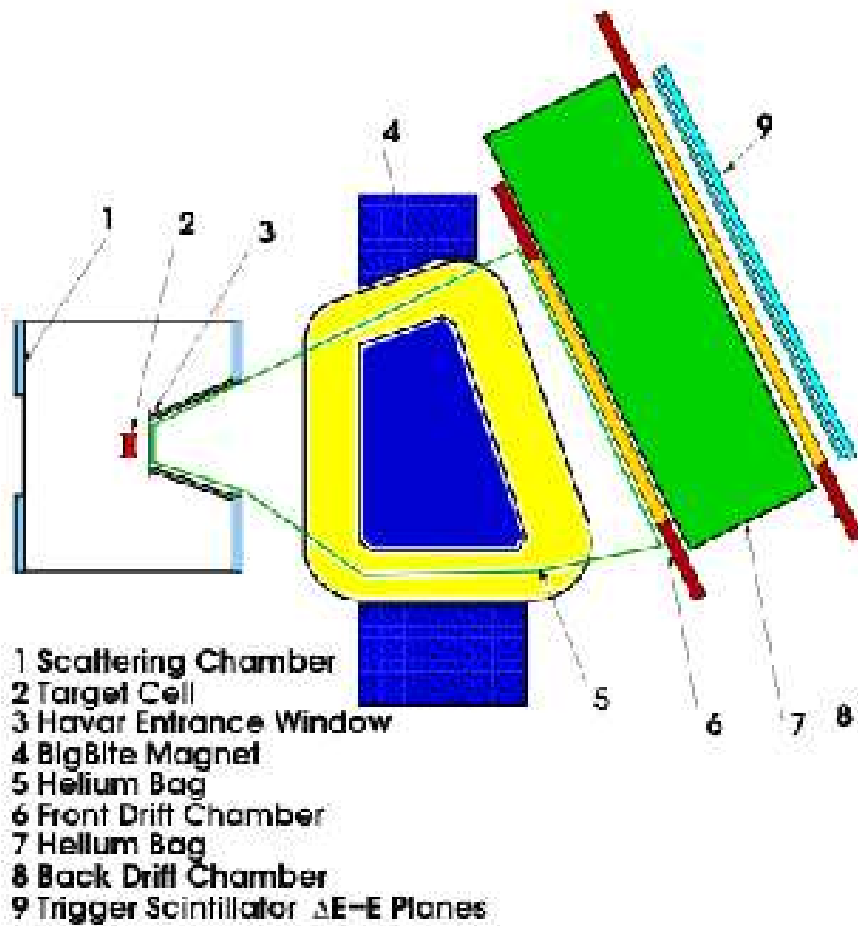


Figure 5: Schematic of the BigBite spectrometer configured for the detection of hadrons. The two helium bags will minimize the multiple scattering of the protons and deuterons. The snout extending towards the target minimizes the area and hence the thickness of the entrance window to the first helium bag. Charged particles are detected by the pair of three-plane wire chambers and the $\Delta E-E$ scintillators.

constant; we change only the value of ϵ_L . The two longitudinal polarizations must differ by a sizable amount but the direction of \vec{q} (the direction of the BigBite) cannot be too far forward or the singles rates will become too high. With the above considerations in mind, we chose (3200 MeV, 12.5°) and (550 MeV, 90.0°). Table 3 lists the major kinematic parameters for these settings, where θ_R is the recoil angle determined by the virtual photon direction, and the relative longitudinal polarization ϵ_L is obtained by Eq. 2.

E (MeV)	θ_e (HRS) (deg.)	Q^2 (fm^{-2})	θ_R (BB) (deg.)	ϵ_L
3200	12.5	12.0	72.8	0.976
550	90.0	12.0	37.3	0.344

Table 3: Kinematic conditions for L/T separation.

The overlap between the finite acceptances of the two spectrometers defines the kinematic space to be covered by the proposed measurements. Fig. 6 shows the covered region for each of the two kinematic conditions *as defined by the HRS*. The area bounded by the solid line is the region covered in the higher energy (3200 MeV, 12.5°) measurements while the area bounded by the combination of dotted and solid lines is the region covered in the lower energy (550 MeV, 90.0°) measurements. The interference terms will be extracted from data taken with the higher electron energy due to the larger cross sections. Consequently, these terms will sample a larger Q^2 range from 10 to 13.2 fm^{-2} . At the lower electron energy the measurements will cover a narrower Q^2 range from 11.6 to 12.2 fm^{-2} .

Fig. 7 shows the dependence of the kinetic energy of the proton on the laboratory angle θ_q of the proton relative to the virtual photon direction at $Q^2 = 12 fm^{-2}$. The radially dashed curves represent the CM polar angle θ_p , ranging from 10° to 170° clockwise. The most energetic protons are emitted at a CM angle of $\theta_p = 0^\circ$; for $E_{np} = 8 MeV$ they have a kinetic energy of 98 MeV, corresponding to a momentum of 440 MeV/c . The corresponding least energetic proton (for $\theta_p=180^\circ$ in the CM frame) has an energy of 35

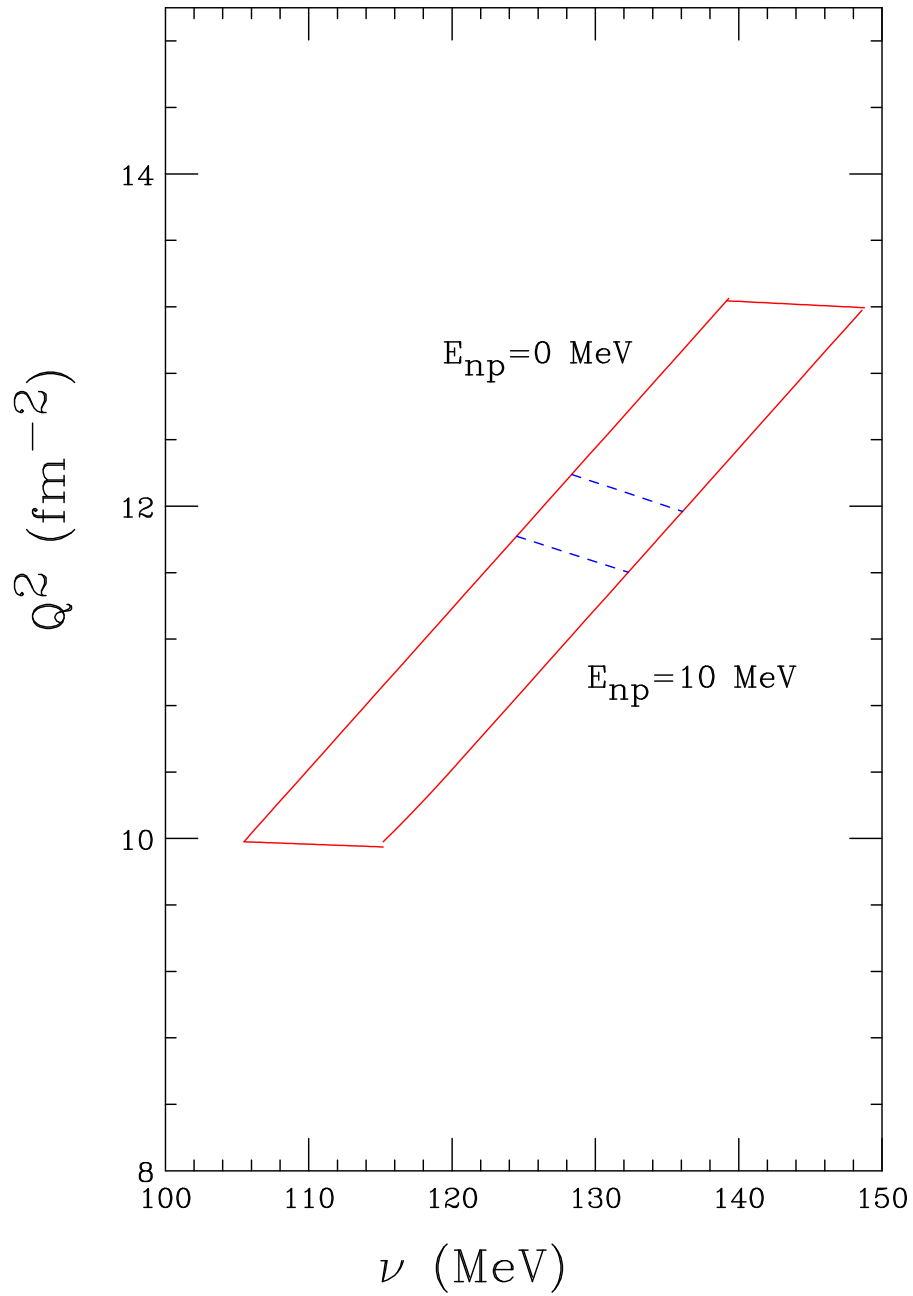


Figure 6: $Q^2 - \nu$ phase space coverage as defined by the HRS. The area bounded by the solid (red) line is the region covered in the higher energy (3200 MeV, 12.5°) measurements while the area bounded by the combination of dashed (blue) and solid lines is the region covered in the lower energy (550 MeV, 90.0°) measurements.

MeV and is also emitted at $\theta_q = 0^\circ$. These momenta easily fall within the acceptance of the BigBite spectrometer.

If the BigBite spectrometer is centered on the nominal direction of \vec{q} then only protons emitted at θ_p from 0° to 50° and from 140° to 180° will be detected when $E_{np} = 2 \text{ MeV}$. However, if two spectrometer positions are used for each HRS setting and the running time divided between the two configurations, then data will be taken for all values of θ_p and ϕ_p up to $E_{np} = 4 \text{ MeV}$ at $Q^2 = 12 \text{ fm}^{-2}$. We therefore plan to take data with the BigBite positioned along either side of the nominal direction of \vec{q} for each of the two HRS settings.

4.4 Calibration of BigBite

A detailed plan for BigBite calibration is described in ref. [45], Proposal 04-007 “Precision Measurement of π^0 at Threshold: A Test of Chiral QCD Dynamics”. The calibration reaction will be elastic scattering from hydrogen in a CH_2 target. Similarly, the momentum calibration of the BigBite will be determined with a precision of 0.5%.

By the time the proposed experiment runs, the BigBite spectrometer will have been well calibrated during earlier experiments. In particular, the π^0 electroproduction experiment will involve the detection of protons with approximately the same energies as this experiment. Thus, we will have only to confirm the calibrations of the angular precision and the momentum resolution. For this purpose we will use elastic scattering from the proton with a beam energy of 2400 MeV, an electron scattering angle of 12.5° , and the BigBite spectrometer positioned at 67.8° (in position for the first $d(\vec{e}, e'p)n$ kinematics setting). The recoiling proton will emerge at 69° with a momentum of 530 MeV/c, well within the acceptance of the BigBite spectrometer.

Near threshold, the momentum of a deuteron recoiling from an elastic scattering event is approximately twice that of protons from electrodisintegration. These recoiling deuterons will be used as an online calibration of the BigBite detector since they can easily be separated from the protons by either

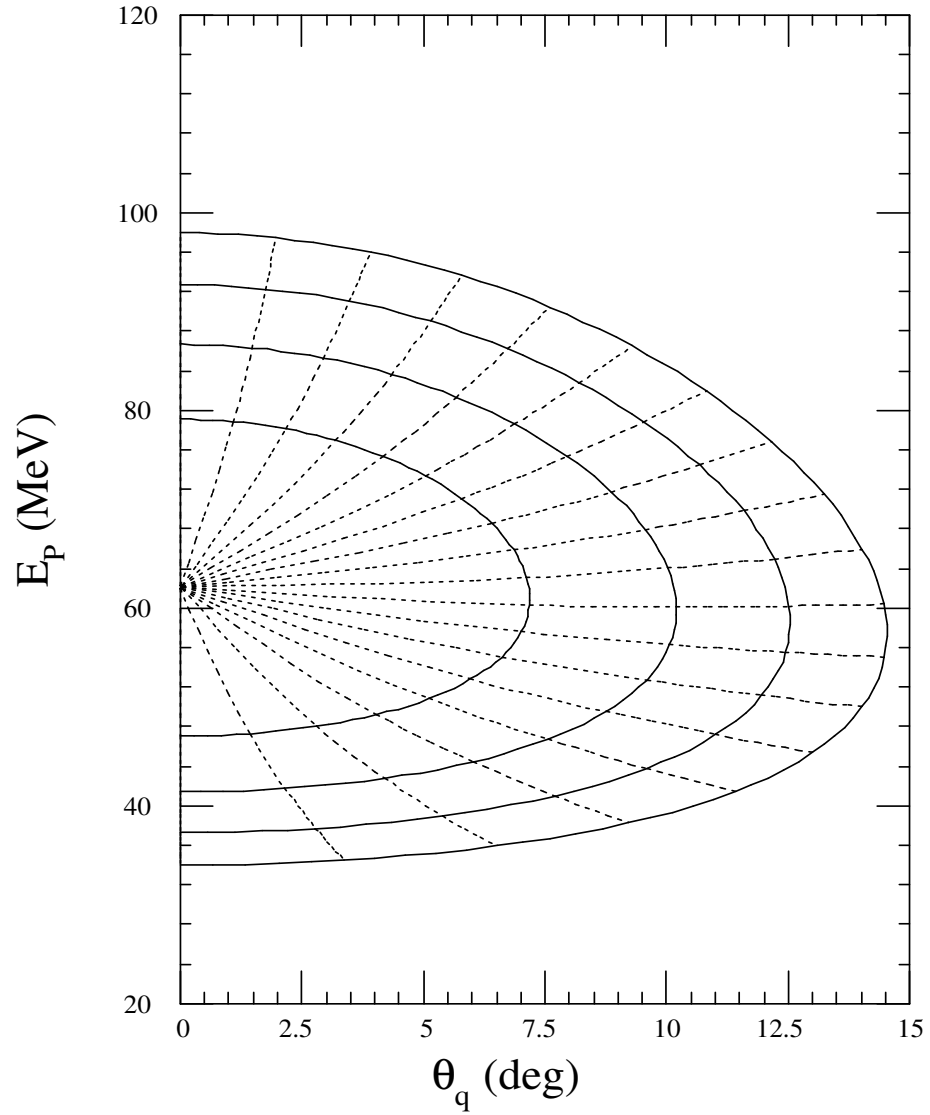


Figure 7: Proton kinetic energy dependence on the polar angle relative to the virtual photon in the laboratory system for $Q^2=12 \text{ fm}^{-2}$ and $E_{np}= 2 \text{ MeV}$ to 8 MeV . The dashed curves label the CM polar angle of the proton from 10° to 170° .

time-of-flight (TOF) or $E-dE/dx$ characteristics.

5 Experimental Simulation

5.1 Resolution

The major kinematic variables such as Q^2 , W , θ_e , and hence E_{np} are determined by the electron arm. The direction of \vec{q} to which the proton is referenced is also derived from these quantities. The resolution in Q^2 and W obtained for $E = 3200 \text{ MeV}$ and $\theta = 12.5^\circ$ by running the Monte Carlo simulation code MCEEP [46], is shown in Fig. 8. The Full Width at Half Maximum (FWHM) for W is 0.63 MeV. According to [46], MCEEP underestimates the resolution about a factor of two. However, it is assumed in the MCEEP code that the HRS is air coupled to the scattering chamber whereas we plan to use a vacuum coupling. Therefore, it can be expected that the E_{np} resolution will be better than the 1.3 MeV indicated by the MCEEP calculation. The electron energy loss will be measured with respect to the deuteron elastic peak, thus limiting the systematic uncertainty in W to less than the aforementioned instrumental uncertainty. Moreover, by referencing to the deuteron elastic peak we limit the effect of uncertainties in the absolute beam energy and HRS momentum resolution to a small change in Q^2 .

The proton arm was simulated (assuming $E = 3200 \text{ MeV}$, $\theta = 12.5^\circ$, $\theta_{BB} = 72.8^\circ$) using a code written by V. Nelyubin [45]. The excitation energy E_{np} was spread between 3 and 5 MeV. Fig. 9 shows the resolution of the polar and azimuthal angle of the proton momentum in the CM system. With the predicted angular resolution, it is practical to choose a bin size of 20° for both θ_p and ϕ_p .

5.2 Systematic Uncertainties

Under the heading of systematic or non-statistical uncertainties we include four groups. First, there are uncertainties in our knowledge of the acceptance of the BigBite spectrometer. Since this will be measured *in situ* using the deuteron elastic scattering events and will be continuously monitored we estimate that it will introduce only about a 2% “acceptance” uncertainty;

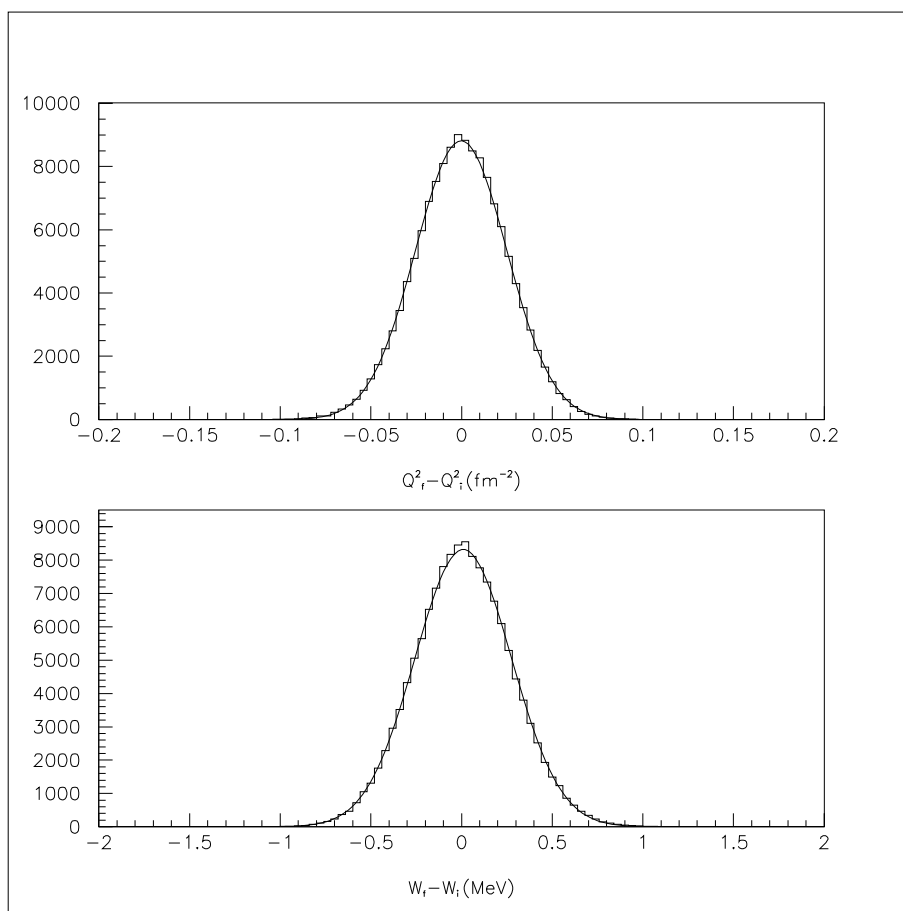


Figure 8: Resolution of Q^2 , W at 3200 MeV and 12.5°

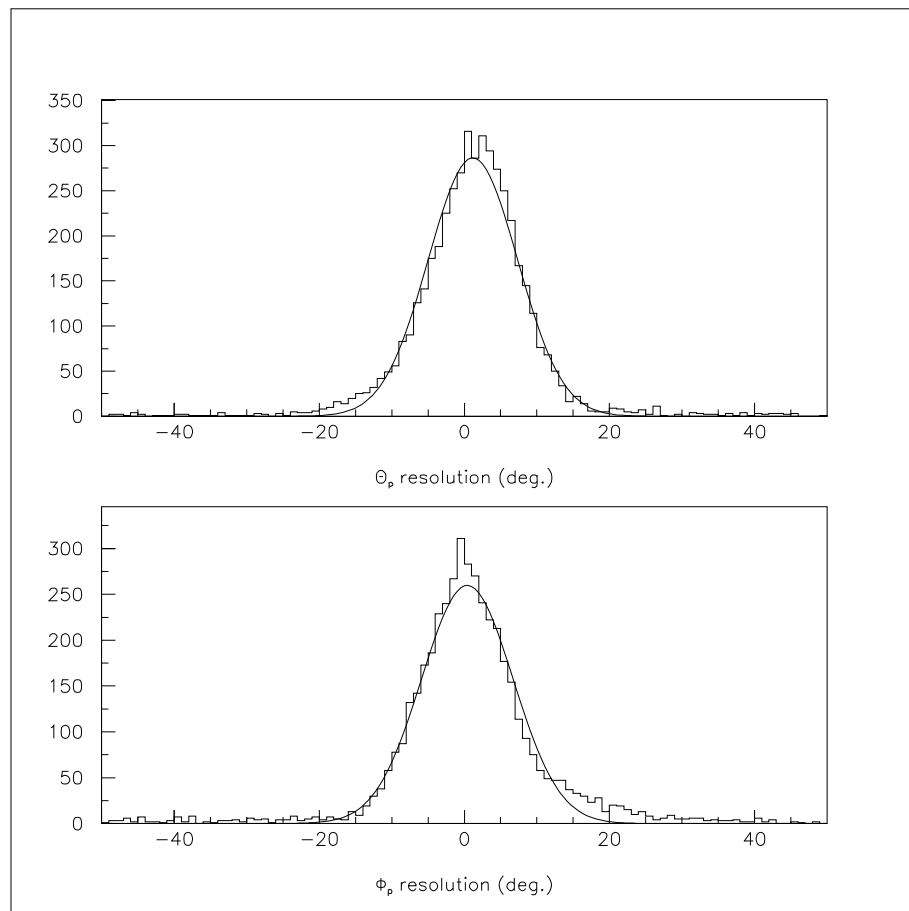


Figure 9: Resolution of θ_p , ϕ_p in CM system.

less for low values of E_{np} , somewhat more for high values of E_{np} . Second, there are the effects of the momentum and angular resolutions of the HRS. Because the cross sections are strong functions of both electron energy and angle these can cause a “skewing” of the results. In principle, these effects can be removed but we have not investigated the degree to which this is possible so we assume that we could remove only 50% of their effect, leaving a residual uncertainty of about 1%. We list them as a “resolution” uncertainty. In our calculations we assumed FWHM values of 1×10^{-4} for $\delta E'/E'$ and 2 mrad for $\delta\theta_e$. Third, there is the uncertainty in our knowledge of the beam current and target thickness. These combine to produce a “normalization” uncertainty of 2%. One would hope that any systematic error in the beam current and target thickness would be the same for both the forward and backward angle data. However, in determining the effects of this “normalization” uncertainty in our extraction of f_L and f_T we have conservatively assumed that the two data sets have statistically independent “normalization” uncertainties and we have added their effects in quadrature. Fourth, there are the “absolute” uncertainties associated with our absolute knowledge of the electron beam energy, $\delta E/E$ ($=2 \times 10^{-4}$) and of the central angle of the HRS, $\delta\theta_{HRS}$ ($=0.2$ mrad). These also are expected to contribute at the level about 1%.

Significantly, uncertainties in the positioning and absolute momentum setting of the BigBite spectrometer have not been listed. There are two reasons for this. First, we will measure simultaneously the kinematically over determined $d(e,e'd)$ reaction. All determination of proton momentum will be made with respect to this fiducial. Second, we will employ the technique which was used to calibrate 180° electron scattering systems at the MIT-Bates Laboratory [47] and elsewhere. We will select electron events in the HRS for which the direction of \vec{q} is the same but for which E_{np} ranges from 0 MeV to some finite value. The phase space factors in Eq. 1 make the cross section rise quickly as E_{np} increases from 0 MeV, independent (for small E_{np}) of azimuthal angle. Consequently, the distribution of protons as a function of the angle between their momenta and \vec{q} will be a parabola centered on \vec{q} . Similarly their energies will be distributed in a predictable pattern about a value calculable from the electron kinematics. The error in the calibration of the direction of \vec{q} was estimated by simulating a representative distribution of protons generated by monochromatic electrons scattering (nominally) through a fixed angle with a fixed energy loss; the actual scattering angle and energy loss were varied

according to the HRS resolutions. A simple fit of the angle and momenta of the recoiling protons yielded a measure of the \vec{q} direction within about 0.3 mrad, a little more than the electron energy or angle. Thus, as in the case of 180° electron scattering we will use the data themselves to calibrate the data.

In evaluating the effects of systematic or non-statistical uncertainties upon the extracted quantities one must note 1) that the dependence of the determinations of the interference structure functions, f_{LT} , f_{TT} , and f'_{LT} , on systematic uncertainties differs greatly from that of the Rosenbluth extraction of f_L and f_T and 2) that the direction of \vec{q} is determined solely by the electron kinematics. Since the interference structure functions, f_{LT} , f_{TT} , and f'_{LT} are determined from the distribution of protons about \vec{q} the systematic uncertainties associated with them come mainly from the multiplicative acceptance and normalization uncertainties. These combine to give a systematic uncertainty of about 4%. For the longitudinal and transverse structure functions extracted from a Rosenbluth separation, the effects of the systematic uncertainties were determined by applying them separately to each of the forward and backward angle measurements and then extracting f_L and f_T . The results of this calculation are shown in table 4.

	Resolution (%)	Normalization (%)	Absolute (%)
δf_L	2.1	5.3	1.0
δf_T	2.8	5.7	1.0

Table 4: Effects of systematic uncertainties in the Rosenbluth separation of f_L and f_T . The absolute contribution is from the uncertainty of beam energy, central angle of the HRS. The normalization uncertainty includes the target thickness and the beam current measurement. The resolution effect is from instrumentation.

5.3 Backgrounds and Accidental Coincidences

The kinematics of the proposed measurements involve the highest energy scattered electrons possible from a deuterium target. Consequently, there is no other single process that can generate an (e,p) or (e,d) coincidence that could be mistaken for an event of interest. Figure 10 shows, for measurements at (3200 MeV, 12.5°) the distribution of electron energies versus scattering angle within the HRS acceptance for the first three processes: elastic scattering, electrodisintegration ($E_{np} = 0$ MeV and 10 MeV), and quasi-elastic scattering. The cross sections for these three processes under these kinematics are

$$\begin{aligned}
 \text{p elastic} & \approx 1 \times 10^{-30} \text{ cm}^2/\text{sr}, \\
 \text{d elastic} & \approx 2 \times 10^{-33} \text{ cm}^2/\text{sr}, \text{ and} \\
 \text{d electrodisintegration} & \approx 1 \times 10^{-33} \text{ cm}^2/\text{sr} \text{ (depends on } E_{np}^{max}\text{)}.
 \end{aligned}$$

Thus, the counting rate in the HRS for quasi-elastic scattering will dominate by a factor greater than 300 the rates of the other processes. We plan, therefore, to replace the S_0 scintillator by one that will cover only the lower (higher electron energy) region of the focal plane with its upper edge angled so that electrons with energies above the indicated dashed line in fig. 10 will trigger it. We could, if necessary, tune the HRS magnet such that lower energy electrons from QE scattering will not strike the detectors. However, we would prefer to have the electrons from electrodisintegration and elastic scattering events strike the center of the focal plane where the resolution is the best.

Accidental coincidences between products of different reaction events are not a significant concern. The elastic $d(e, e'd)$ reaction is complete so knowledge of the electron kinematics, measured precisely in the HRS, dictate where the corresponding deuteron must be. In the case of the $d(\vec{e}, e'p)n$ reaction, knowledge of the electron kinematics defines the cone within which corresponding protons must emerge. And, for each direction within the cone only two momenta are possible for the proton. Consequently, accidental coincidences will be severely suppressed.

The principal potential concern with respect to rates/backgrounds is the

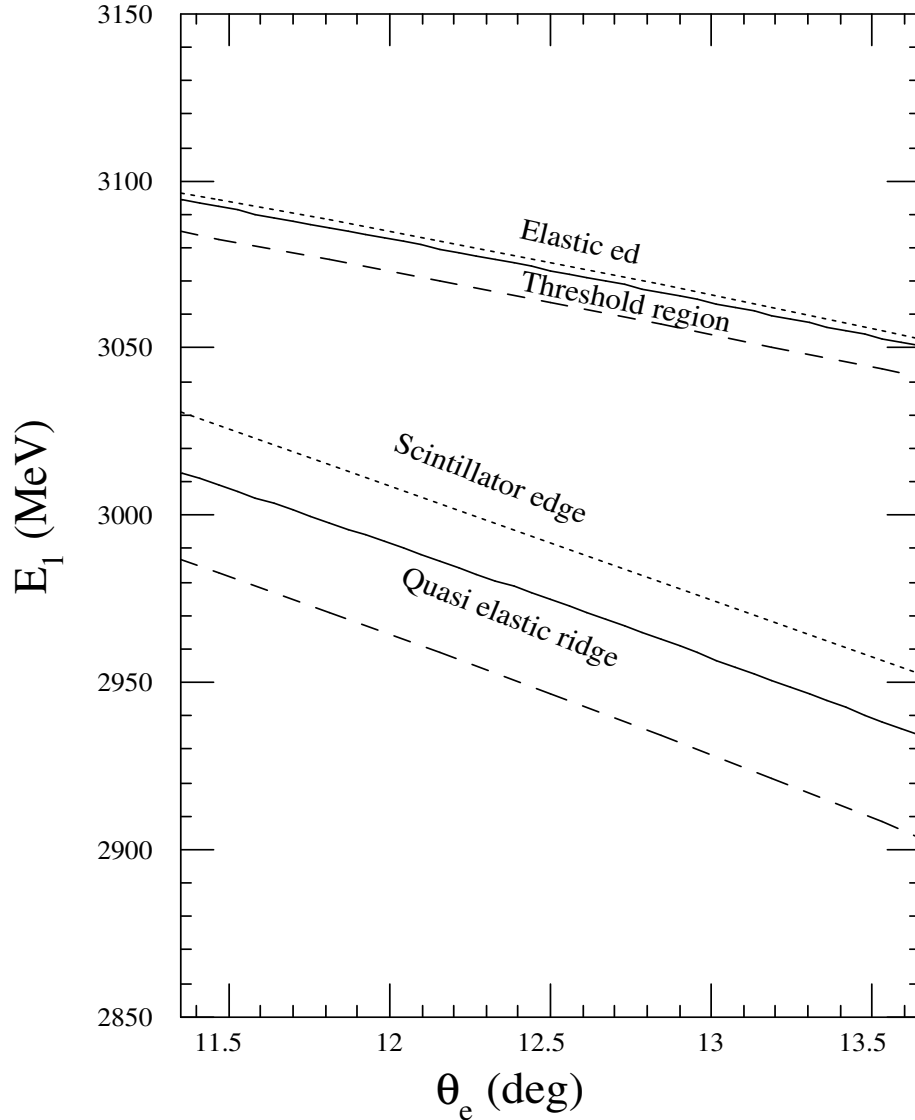


Figure 10: Distribution of electrons on the HRS focal plane. Electrons from elastic (upper short-dashed line) and threshold electrodisintegration events (upper solid line - $E_{np} = 0$ MeV, upper long-dashed line - $E_{np} = 10$ MeV) are clearly separated from those coming from quasi-elastic events. The lower long-dashed (solid) line indicates the electron energy corresponding to a scattering from a proton with initial momentum equal to the Fermi momentum anti-parallel (parallel) to \vec{q} . A scintillator with its upper edge (corresponding to lower energy) as indicated by the short-dashed line will enable us to reduce the singles rate in the HRS by accepting only events in which an electron triggers this scintillator.

singles rates in the wire chambers of the BigBite spectrometer. During the GEn experiment it was observed that an effective “total luminosity” of 0.5×10^{37} was the maximum usable. At this level the instantaneous rate in the wirechambers was about 20 MHz corresponding to a per-wire rate of approximately 150-200 kHz, or about 4 kHz/cm. We plan to run at a luminosity of 3×10^{37} , a factor of 6 higher. To understand how we will be able to run at this luminosity we must consider both the source of these events and how these rates limit the experiment [48].

In the GEn experiment, the instantaneous rate was dominated by random events in individual chambers. These were traced to a high flux of low energy photons producing low energy electrons either shortly before or within a wire chamber. For each valid trigger a large number of events were recorded in the wire chambers. Reconstructing the valid tracks of 1+ GeV electrons required searching through a large number of combinations of events in the front and rear chambers. At a total luminosity of 0.5×10^{37} nucleons/cm²/s the track reconstruction efficiency was about 75% and the computational demands were approaching practical limits. In the proposed experiment, we will have three advantages in this regard:

- the reaction vertex will be isolated to within less than 1 cm due to the high precision of the HRS used to detect the scattered electron;
- the direction of the momentum transfer vector will be precisely known so the direction of emitted protons or deuterons will be tightly constrained. In the case of the protons from $d(\vec{e}, e'p)n$, knowledge of where they strike the first chamber severely constrains where they must strike the second chamber;
- the momenta of the particles of interest (p, d) are at least a factor of 2 lower than the momenta of electrons detected in the GEn experiment. This means the curvature of their tracks will be at least a factor of 2 tighter, making the sensitivity of their position at the second chamber with respect to their momenta that much greater; and
- in the GEn experiment the particles of interest in the BigBite spectrometer were electrons. As a result, the thresholds on the chamber

signals had to be set low enough to register these particles. During the proposed experiment the relatively low momentum protons and deuterons to be detected in the BigBite spectrometer will deposit significantly more energy in each chamber than do minimally ionizing electrons. We will, therefore, raise the thresholds on the chambers to minimize their sensitivity to electrons. Even if we are overly careful so as to ensure that none of the highest energy protons of interest are lost, we conservatively estimate that raising these thresholds will reduce the singles rate due to electrons by at least a factor of two.

Consequently, we are confident that track reconstruction issues will not limit the proposed experiment.

The overall singles rates in the BigBite wire chambers during the GEN experiment were high, but within the capability of the chambers to handle without undue loss of efficiency. The per-channel readout rate of less than 200 kHz posed no special problem. Similar chambers performed equally well at comparable rates during the Hall C hypernuclear experiment.

Three factors lead us to conclude that we can achieve a singles rate approximately equal to that observed in the GEN experiment despite the higher luminosity:

- The target used in the GEN experiment was the 40-cm long polarized ^3He cell with entrance and exit windows of thicknesses comparable to the target material and necessarily very open geometry. It was observed during that experiment that about 1/3 of the backgrounds did not come directly from the target, but from surrounding material from which there was a line-of-sight path to the detectors. We will use the standard scattering chamber with a snout constructed of 1 inch thick aluminum extending almost to the target cell. The snout will be designed similarly to the one to be used in the threshold π^0 electroproduction experiment and will mask the end caps of the target cell. The target cell will be the 6 cm long cell being constructed for the threshold π^0 experiment. Additional shielding as needed will be placed around the chamber. These changes should reduce the backgrounds by a factor of two thirds.

- A shielding hut for the BigBite detector package is currently under design [49] and will be available when the proposed experiment runs. It will consist of plates of steel 0.5 inches thick on all four sides and, if necessary, the top of the detectors. It is anticipated based on previous experience that this will result in approximately a factor of two reduction in background rate.
- Helium bags will be inserted between the target and the first chamber as well as between the two chambers. Inasmuch as this will reduce the electron density in front of the chambers by a factor of about 7 over air, it will greatly reduce the flux of electrons from this region. It should be noted that helium gas was flowed around the target during the GEn experiment so the advantage to be realized in comparison to that experiment will be less. Nevertheless, we can expect that an improvement of about a factor of two can be realized.

Combining these factors alone, we expect a singles rate in the BigBite spectrometer on the order of $(2/3 \times 1/2 \times 1/2 \times 12 \times 20 \text{ MHz} =) 40 \text{ MHz}$. By increasing the detector thresholds to exclude at least a large fraction of the minimally ionizing particles will reduce the rates to or below the levels of the GEn experiment.

Maintaining a relatively high efficiency and, more importantly, monitoring the value of that efficiency will be necessary to obtain the desired precision in the proposed experiment. For this reason, time will be devoted specifically to measuring rates as a function of luminosity. In this regard it should be noted that similar chambers were constructed and used at KVI with similar rates of energy deposition [50]. Stable efficiencies of greater than 95% were measured to a precision of better than 0.5%. Moreover, since the high rates in the BigBite spectrometer are primarily due to low energy photons which strike the chambers uniformly any deterioration of efficiency will be much more uniform than was the case at KVI. Consequently, the KVI experience as well gives us confidence that we can make a precise measurement.

It should also be noted that the deuteron elastic cross section is well known at this momentum transfer. Figure 11 (taken from ref. [51]) shows existing data for the elastic structure function $A(Q^2)$. For the momentum transfer of the

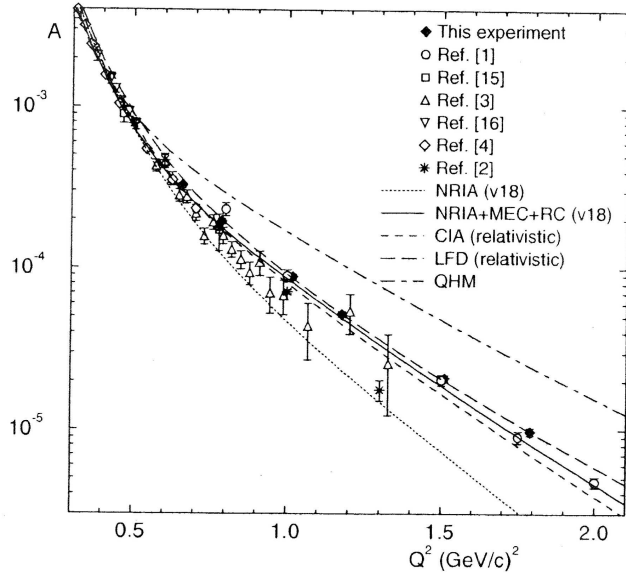


Figure 11: Existing data for the elastic structure function $A(Q^2)$. Figure was taken directly from ref. [51]. References listed in the figure refer to references in that article. Note that for the momentum transfer of the proposed measurement [$Q^2 = 0.47 (GeV/c)^2$] the data are consistent at the few percent level and well reproduced by theory.

proposed measurement [$Q^2 = 0.47 (GeV/c)^2$] the data are consistent at the few percent level and well reproduced by theory. Consequently, the results for the separate structure functions for $d(\vec{e}, e'p)n$ can be normalized to this cross section, thereby minimizing the impact of detection efficiencies. While it is our intention to make the best possible absolute measurement, such normalized structure functions would be almost as valuable for dissecting the various contributions within the context of a given model.

After removing the quasi-elastic, Δ , etc. electrons the remaining rate in the HRS will be not more than 2 kHz. With a coincidence window of 40 ns, one obtains an accidental coincidence rate of about 250 Hz, well within the

capabilities of the data acquisition system. The rates for the backward angle measurements will be much lower.

PAC22 recommended that “The experimenters should demonstrate that this experiment can be run within a factor of two of the stated luminosity.” We requested beam time to make direct measurements under representative conditions but were unable to be accommodated due to the tight schedule of experiments. However, we believe that the above reasonable extrapolations from experience constitute a sufficient demonstration. The upcoming $p(e, e'p)\pi^0$ measurement will be performed under conditions very similar to those proposed here. We fully anticipate learning a great deal from that experiment which will enable us to make the proposed experiment even more effective.

5.4 Rate Estimate

To get an estimate of the precision in the final observables, we use the cross section formulas in Eq. 1 and the full calculation from Arenhövel at $E_{np} = 2$ MeV as shown in Fig. 3. The rate shown in Table 5 is based on a 6 cm long deuterium target and 15 μA beam current ($\mathcal{L} = 3 \times 10^{37}/cm^2/s$). The solid angle of the HRS is taken to be 6 msr.

E (MeV)	θ_e (deg.)	Q^2 (fm ⁻²)	$\frac{d\sigma}{d\Omega_e dW}$ (fm ² /sr/MeV)	rate (1/s)
3200	12.5	12.0	3.96×10^{-8}	144
550	90.0	12.0	1.04×10^{-9}	3.8

Table 5: Rate estimate for each HRS setting at $E_{np} = 2 \pm 1$ MeV.

The high energy forward angle setting covers a larger kinematic region. Hence, the effective counting rate for data useful in the L/T separation should be divided by a factor of 6. Table 6 lists the total counts for 96

hours (4 days) of running at high energy and 48 hours (2 days) at low energy. Since the BigBite will have two placements for each HRS setting, the total beam time will be twice this.

For an 8-day run at high energy with two BigBite settings, approximately 8.3×10^6 events will be accumulated in each 2 MeV E_{np} and $0.6 \text{ fm}^{-2} Q^2$ bin. Since the longitudinal and the transverse components of the structure functions are more than one order larger than the interference terms, to reach the same precision, the counts at low energy can be dropped one order down to that at high energy. For a 4-day run at 550 MeV, approximately 0.64×10^6 events will be accumulated in each E_{np} bin.

E (MeV)	θ_e (deg.)	rate (1/s)	beam time (hour)	counts (M)
3200	12.5	13	96	8.3
550	90.0	3.8	48	0.64

Table 6: Projected data for 2 MeV bins in E_{np} and 0.6 fm^{-2} bin for Q^2 .

We will also collect approximately 80×10^6 (0.8×10^6) deuteron elastic events during the higher (lower) energy run. This large number of kinematically over-determined events will be useful as a means of on-line calibration.

5.5 Projected Results

Using the full (Normal+MEC+IC+RC) calculation of Arenhövel as the generating function the experiment was simulated. The interference structure functions were extracted using the data at $E_{np} = 2 \pm 1$ MeV, 3200 MeV beam and 12.5° HRS angle. The longitudinal and transverse structure functions were extracted using the data from the restricted range of Q^2 measured at both 12.5° and 90° . Figure 12 shows the simulated data for f_{LT} atop the calculation of Arenhövel. The error bars are statistical only; the systematic uncertainty is comparable to the statistical.

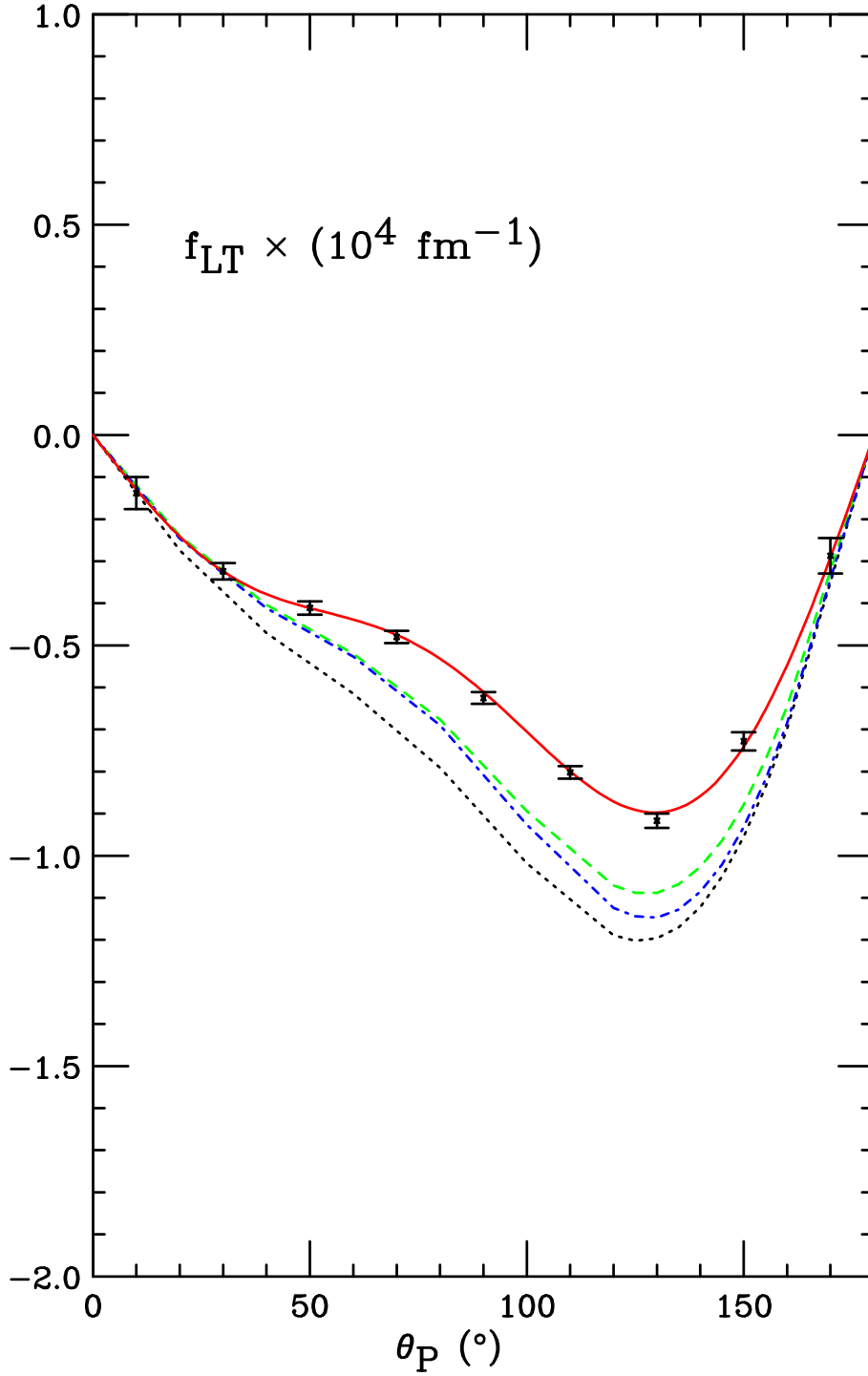


Figure 12: Simulated data at $E_{np} = 2$ MeV. The curves represent the Normal calculation (dotted), the Normal+MEC (dashed), the Normal+MEC+IC (dash-dotted), and the Normal+MEC+IC+RC calculation (solid). The data span the range in Q^2 from 10 to 13.2 fm^{-2} .

Figure 13 shows the simulated data for f_{TT} and f'_{LT} . The error bars are statistical only; in this case the systematic uncertainty is smaller than the statistical.

To simulate the separation of the longitudinal from the transverse structure functions, we used 8.3 M events from 3200 MeV, and 0.64 M events from 550 MeV, since the Q^2 range is limited by the low energy set up. Figure 14 shows the simulated f_T and f_L . The statistical error bars are smaller than the systematic uncertainty.

Compared to the high quality of the data for f_L , f_T and f_{LT} ; f'_{LT} and f_{TT} will be measured with poorer precision. Nevertheless, they will offer measurements of the averaged amplitudes as well as their general shapes.

The data from this experiment will be the first comprehensive set of high quality measurements of threshold deuteron electrodisintegration under kinematic conditions where non-nucleonic degrees of freedom are expected to play major roles. The selectivity of the different structure functions to each non-nucleonic effect provides a powerful tool to focus on each component. It will also be the first set of electrodisintegration data to be obtained simultaneously with elastic scattering data, thus permitting a precise comparison of the two closely related reactions.

5.6 Beam Time Request

Table 7 lists beam time distribution for each kinematic condition. θ_{HRS} and θ_{BB} are the orientation angles of the HRS and BigBite spectrometers respectively. The data from part I will provide the three interference structure functions; the purpose of the part II run is to perform a Rosenbluth separation of f_L and f_T . We request 18 days of beam time, 12 days for data acquisition, 4 days for auxiliary set up, and 2 days for detector rate and background studies.

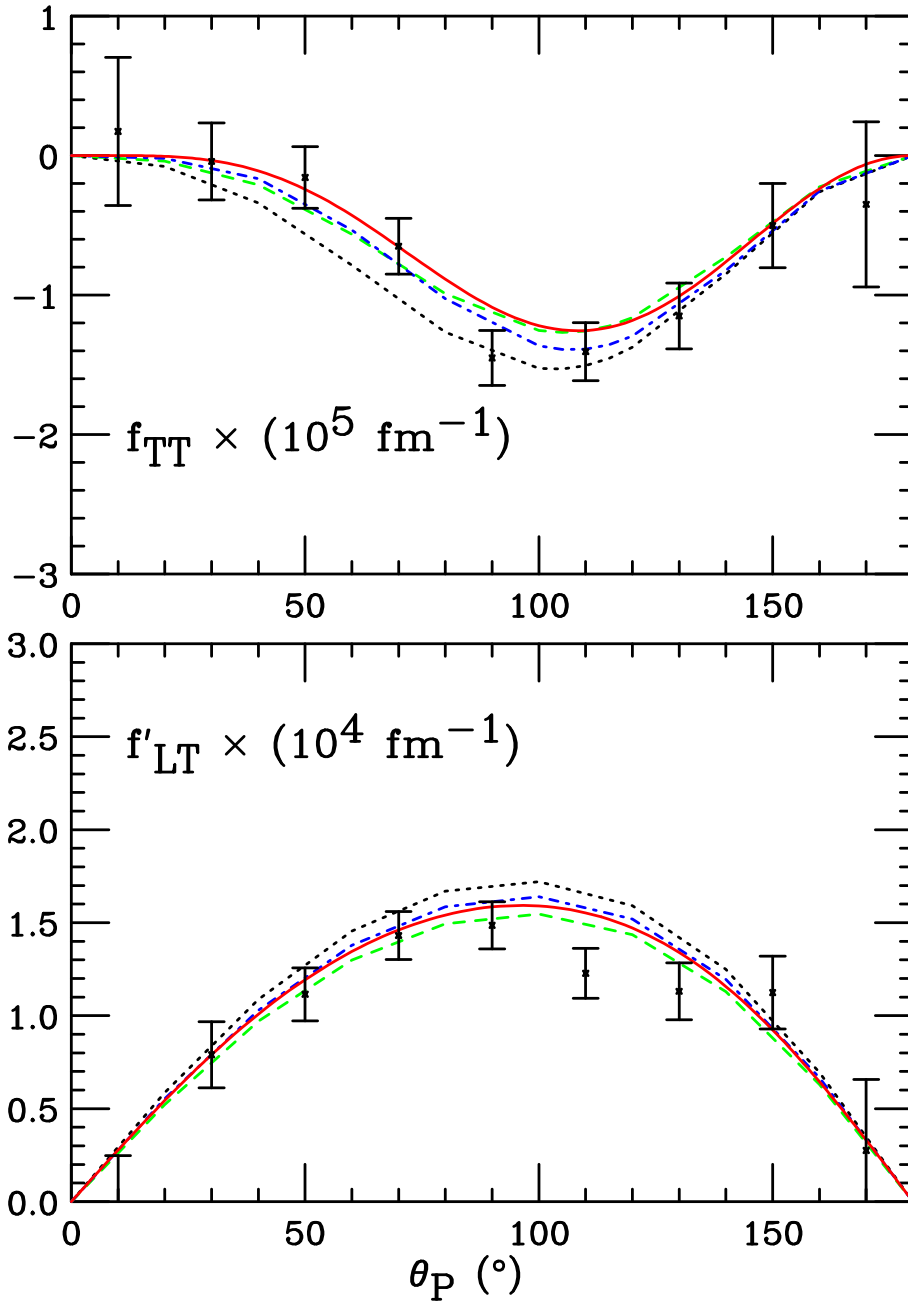


Figure 13: Simulated data at $E_{np} = 2$ MeV. The curves represent the Normal calculation (dotted), the Normal+MEC (dashed), the Normal+MEC+IC (dash-dotted), and the Normal+MEC+IC+RC calculation (solid). The data span the range in Q^2 from 10 to 13.2 fm^{-2} .

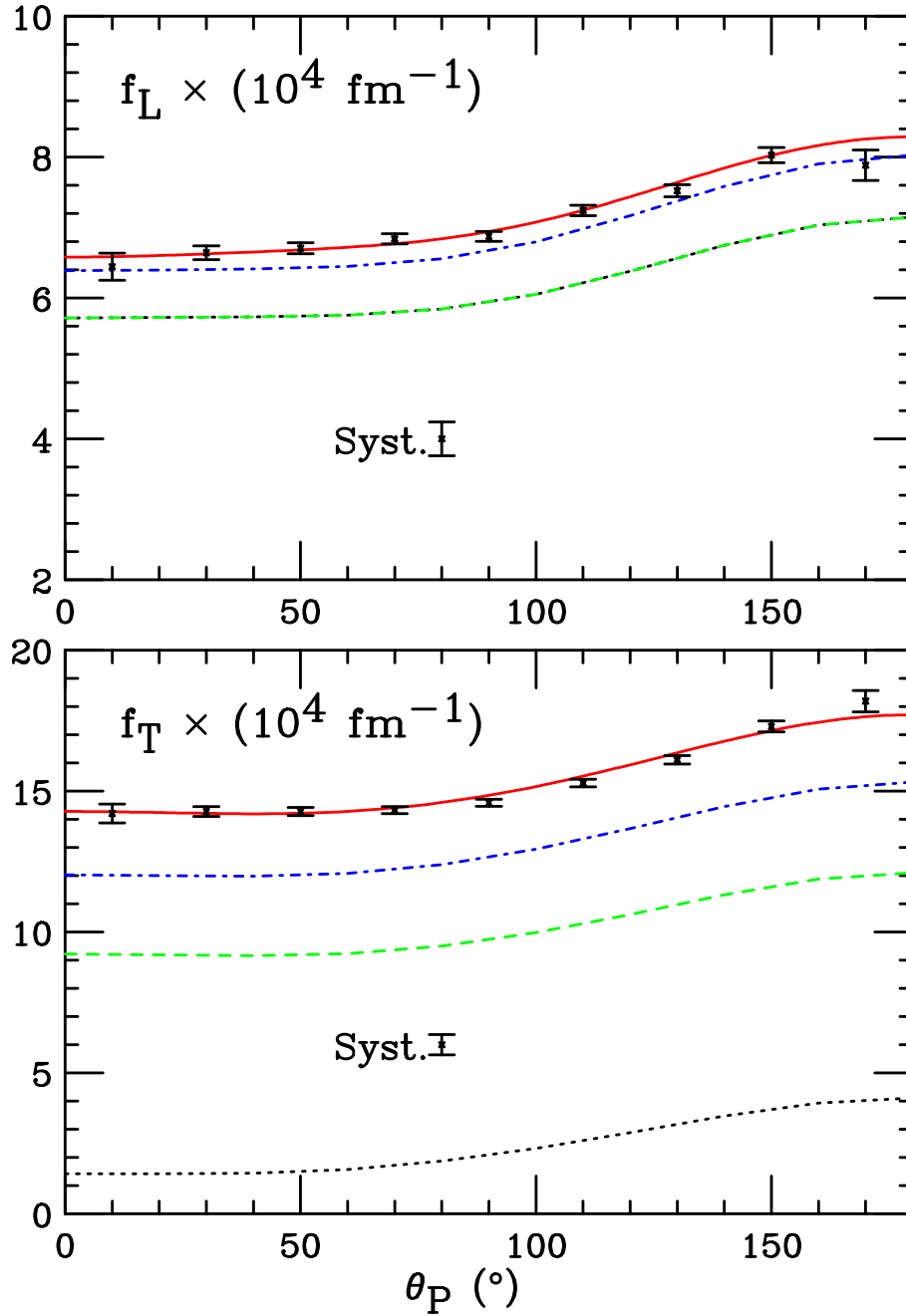


Figure 14: Simulated data at $E_{np} = 2$ MeV. The curves represent the Normal calculation (dotted), the Normal+MEC (dashed), the Normal+MEC+IC (dash-dotted), and the Normal+MEC+IC+RC calculation (solid). The error bars reflect data at Q^2 from 11.6 to 12.2 fm^{-2}

	E (MeV)	θ_{HRS} (deg.)	θ_{BB} (deg.)	target	time (hour)
part I	3200	12.5	67.8	LD ₂	96
	3200	12.5	77.8	LD ₂	96
part II	550	90.0	32.3	LD ₂	48
	550	90.0	42.3	LD ₂	48
subtotal					288
calibration	2400	12.5	67.8	LH ₂	12
energy change (2)					12
detector move (3)					48
detector tuning					24
rates & bkgd studies					48
subtotal					144
total					432

Table 7: Beam time requested.

6 Summary

We propose an exclusive study of the reaction $d(\vec{e}, e'p)n$ at $Q^2 = 12 \text{ fm}^{-2}$ and $E_{np} = 2$ to 8 MeV in Hall A with the HRS and BigBite spectrometers. Deuteron elastic scattering will be measured simultaneously. We request 16 days of beam time, of which 12 days will be for data acquisition and 4 days for detector placement and calibration. This will be the first systematic measurement of near threshold electrodisintegration of the deuteron in out-of-plane kinematics at a momentum transfer Q^2 where non-nucleonic degrees of freedom are expected to play major roles.

The proposed measurements will provide a new set of benchmarks against which nucleon-nucleon interaction calculations can be tested to a higher level.

References

- [1] PAC 14 Few-Body Workshop, Willimasburg, July, 1998.
- [2] S. Auffret *et al.*, Phys. Rev. Lett. **55**, 1362 (1985).
- [3] B. Mosconi and P. Ricci, Nucl. Phys. **A517**, 483 (1990).
- [4] F. Ritz *et al.*, Phys. Rev. C **55**, 2214 (1997).
- [5] G. van der Steenhoven *et al.*, in AIP Conf. Proc 243, P793, 1991.
- [6] W. Kasdorp *et al.*, Phys. Lett. B **393**, 42 (1997).
- [7] F. Frommberger *et al.*, Phys. Lett. B **339**, 17 (1994).
- [8] H. Arenhovel, Few-Body Sys., Suppl **6**, 206 (1992), and references therein.
- [9] R. Schiavilla, Phys. Rev. C **72**, 034001 (2005).
- [10] B. Sawatzky, PhD dissertation, University of Virginia, 2005.
- [11] M. Blackston, PhD dissertation, Duke, 2007.
- [12] P. von Neumann-Cosel *et al.*, Phys. Rev. Lett. **88**, 202304 (2002).
- [13] G. Peterson and W. Barber, Phys. Rev. **128**, 812 (1962).
- [14] K. S. Lee *et al.*, Phys. Rev. Lett. **67**, 2634 (1991).
- [15] W. Schmitt *et al.*, Phys. Rev. C **56**, 1687 (1997).
- [16] Y. Antuf'ev *et al.*, Sov. J. Nucl. Phys. **22**, 121 (1976).
- [17] V. Agranovich *et al.*, Sov. J. Nucl. Phys. **25**, 595 (1978).
- [18] M. Bernheim *et al.*, Phys. Lett. **B142**, 145 (1984).
- [19] T. Tamae *et al.*, Phys. Rev. Lett. **59**, 2919 (1987).
- [20] T. Tamae, Proposal to MIT Bates, 1990, 1990, 89-15.

- [21] T. Reichelt *et al.*, in AIP Conf. Proc 243, P794, 1990.
- [22] S. Dolfini *et al.*, Phys. Rev. C **60**, 64622 (1999).
- [23] Z.-L. Zhou *et al.*, Phys. Rev. Lett. **87**, 172301 (2001).
- [24] M. van der Schaar *et al.*, Phys. Rev. Lett. **68**, 776 (1992).
- [25] A. Pellegrino *et al.*, Phys. Rev. Lett. **78**, 4011 (1997).
- [26] D. Jordan *et al.*, Phys. Rev. Lett. **76**, 1579 (1996).
- [27] J. Ducret *et al.*, Phys. Rev. C **49**, 1783 (1994).
- [28] G. Simon *et al.*, Nucl. Phys. **A324**, 277 (1979).
- [29] D. Ganichot *et al.*, Nucl. Phys. **A178**, 545 (1972).
- [30] B. Bodan *et al.*, Nucl. Phys. A **549**, 471 (1992).
- [31] M. van der Schaar *et al.*, Phys. Rev. Lett. **66**, 2855 (1991).
- [32] Z.-L. Zhou, PROC on electronucleon physics with Int target, 1999.
- [33] K. Blomquist *et al.*, Phys. Lett. B **424**, 33 (1998).
- [34] R. Bohm, thesis, Mainz, 2001.
- [35] H. Bulten *et al.*, Phys. Rev. Lett. **74**, 4775 (1995).
- [36] W. Fabian and H. Arenhovel, Nucl. Phys. **A314**, 253 (1979).
- [37] H. Arenhovel, Nucl. Phys. A **384**, 287 (1982).
- [38] M. Bernheim *et al.*, Nucl. Phys. **A365**, 349 (1981).
- [39] J. Laget, Phys. Lett. B **199**, 493 (1987).
- [40] A. Cambi, B. Mosconi, and P. Ricci, Phys. Rev. Lett. **48**, 462 (1982).
- [41] A. Cambi, B. Mosconi, and P. Ricci, Phys. Rev. C **26**, 2358 (1982).
- [42] H. Arenhovel *et al.*, Phys. Rev. C **52**, 1232 (1995).

- [43] E. Hummel and J. Tjon, Phys. Rev. C **49**, 21 (1994).
- [44] H. Arenhovel, private communication, 2001.
- [45] R. Lindgren *et al.*, Proposal to Jlab, 04-007, 2004, unpublished.
- [46] P. Ulmer, Monte Carlo code, private communication, 2002.
- [47] G. Peterson *et al.*, Nucl. Instr. and Meth. **160**, 375 (1979).
- [48] N. Liyanage, private communication, 2007.
- [49] D. Higinbotham, private communication, 2007.
- [50] M. Volkerts *et al.*, Nucl. Instr. and Meth. **A 428**, 432 (1999).
- [51] D. Abbott *et al.*, Phys. Rev. Lett. **82**, 1379 (1999).